REPORT DOCUMENTATION PAGE

Form Approved
OMB No. 074-0188

1. AGENCY USE ONLY (Leave blank)	2. REPORT DATE	3. REPORT TYPE AND DATES COVERED
	12/28/97	Final 11/1/94 - 10/31/97

4. TITLE AND SUBTITLE
Energy transfer processes in Iodine lasers

5. FUNDING NUMBERS
61102F 2303 ES

6. AUTHOR(S)
Michael C. Heaven

7. PERFORMING ORGANIZATION NAME(S) AND ADDRESS(ES)
Emory University
1784 N. Decatur Road
Suite 510
Atlanta, GA 30322

8. PERFORMING ORGANIZATION REPORT NUMBER

9. SPONSORING / MONITORING AGENCY NAME(S) AND ADDRESS(ES)
AFOSR/NC
Building 410,
Bolling AFB
DC 20332-6448

10. SPONSORING / MONITORING AGENCY REPORT NUMBER
F49620-95-1-0010

11. SUPPLEMENTARY NOTES

12a. DISTRIBUTION / AVAILABILITY STATEMENT
APPROVED FOR PUBLIC RELEASE: DISTRIBUTION IS UNLIMITED

12b. DISTRIBUTION CODE

13. ABSTRACT ***(Maximum 200 Words)***

The near resonant electronic energy transfer process $I(^2P_{3/2}) + O_2(a) \leftrightarrow I(^2P_{1/2}) + O_2(X)$ is of central importance in COIL systems. The low temperature kinetics were characterized by studies of $I(^2P_{1/2})+O_2$ quenching at temperatures near 150K. As a component of this effort, sensitive LIF detection of $I(^2P_{1/2})$ was demonstrated. A quenching rate constant of $(4.5\pm0.5)\times10^{-12}$ cm^3 s^{-1} was obtained, which was appreciably smaller than the values used in current computer models. *Ab initio* calculations for $I+O_2$ show that transfer is mediated by potential energy surface crossings that occur at short-range.

Vibrational relaxation of $I_2(X)$ influences the efficiency of COIL systems. Ro-vibrational relaxation rate constants were measured for a range of collision partners (He, Ar, N_2, O_2, Cl_2, I_2, H_2O). Overall, the inelastic collision dynamics were consistent with the predictions of classical trajectory models. Vibrational relaxation at low temperatures (<20 K) was examined in a free-jet expansion.

Energy transfer from $NCl(a)$ to I_2 was examined. Although quenching of $NCl(a)$ was near gas kinetic, preliminary results suggest that E-V transfer is inefficient.

Ab initio calculations for Cl_3, attempts to detect bound trihalogen intermediates, and new spectroscopic data for the D'-A' system of Br_2 are described

14. SUBJECT TERMS
Energy transfer, Chemical lasers, Oygen iodine Laser, COIL

15. NUMBER OF PAGES

16. PRICE CODE

17. SECURITY CLASSIFICATION OF REPORT	18. SECURITY CLASSIFICATION OF THIS PAGE	19. SECURITY CLASSIFICATION OF ABSTRACT	20. LIMITATION OF ABSTRACT
UNCLASSIFIED	UNCLASSIFIED	UNCLASSIFIED	

Contents

1. Introduction and overview.

The chemical oxygen iodine laser (COIL) is now developed to the point where ground-based systems can reliably provide very high output energies. This device relies on energy transfer from $O_2(a)$ to I_2. First the $O_2(a)$ metastables dissociate molecular iodine, then they excite the atomic products to the upper laser level ($I\ ^2P_{1/2}$). The mechanism by which the laser operates involves several types of energy transfer events. Studies of the elementary processes have established rate constants for several key reactions, and yielded valuable insights concerning the principles that govern collisional energy transfer. However, the complexity of the lasing kinetics is formidable. While much progress has been made, a full understanding of the kinetics has not yet been achieved. In particular, questions regarding the temperature dependence of the crucial transfer step

$$O_2(a^1\Delta) + I(^2P_{3/2}) \leftrightarrow O_2(X^3\Sigma^-) + I(^2P_{1/2}) \qquad [1]$$

and the I_2 dissociation mechanism remain to be answered. From a practical perspective, this information is needed for the development of supersonic COIL devices that work at elevated pressures (i.e., above 75 Torr, high pressure operation is desirable for airborne lasers).

In the present studies we examined the temperature dependence of reaction [1] by measuring the I^*+O_2 quenching rate constant at temperatures near 150 K, which corresponds to the typical conditions in a supersonic COIL device. The results indicated that the low temperature forward and reverse transfer rate constants (k_f and k_b) were much smaller than the values used in current kinetic models[1]. It was also found that equations currently used to represent the temperature dependence of the rate constants were not of the correct form[1]. These conclusions were supported by results from an *ab initio* electronic structure investigation of the transfer mechanism.

The dissociation of I_2 in COIL systems involves highly vibrationally excited levels of $I_2(X)$ (denoted by $I_2^\dagger$ in the following). Collisional relaxation of vibrationally excited I_2 therefore influences the overall efficiency of the laser. Knowledge of the vibrational relaxation rate constants is needed for the analysis and design of high pressure COIL devices, as vibrational deactivation may prove to be a limiting factor. In addition, studies of $I_2(X)$ inelastic collision dynamics provide data that can be compared with the corresponding (and far more extensive) data for $I_2(B)$. This comparison is a matter of fundamental interest. $I_2(B)$ has been used as a prototype for studies of ro-vibrational energy transfer for more than 70 years. Although the *B* state is embedded in a manifold of

electronically excited states, the role of non-adiabatic mixing in ro-vibrational energy transfer has not been examined.

We have investigated rotational and vibrational relaxation of $I_2(X)$ levels in the range $23 \leq v \leq 42$[2,3]. The collision partners included species that are present in COIL systems (He, O_2, Cl_2, and H_2O) and possible alternative carrier gases (Ar and N_2). Comparisons with the *B* state dynamics indicated that non-adiabatic effects were present for the excited state. Fortunately, these effects could be easily incorporated into conventional models of ro-vibrational energy transfer. The temperature dependence of $I_2^{\dagger}$ vibrational relaxation rate constants was examined by observing low temperature collisions in a free-jet expansion. These measurements were undertaken to provide data for analysis of supersonic COIL systems, and to search for evidence of enhanced low temperature transfer cross sections resulting from the action of long-range forces and/or resonances.

The electronic to vibrational energy transfer process $I(^2P_{1/2}) + I_2(X, v=0) \rightarrow I(^2P_{3/2}) + I_2(X, v\approx40)$ is a critical chain branching step in the dissociation of I_2 by $O_2(a)$. The unusually high rate constant for this process has been ascribed to transient formation of bound I_3. Bound states of trihalogens have been used to account for a number of kinetic observations, but these species have yet to be definitively characterized. In an attempt to obtain spectroscopic data for trihalogens, we have explored the possibility of generating X_3 radicals in matrices by *in situ* photolysis of HX-X_2 complexes. As there are reports of gas phase spectra that were tentatively ascribed to Cl_3[4,5], we started by trying to isolate this species. Photolysis of HCl/Cl_2/Ar matrices produced a new emission band near 470 nm. This emission was consistent with the gas phase data, and tentatively ascribed to Cl_3[6]. High-level *ab initio* calculations were performed to examine possible assignments for the electronic states involved in the 470 nm band[7]. Unexpectedly, these calculations showed that it was most unlikely that the new matrix spectrum, or the previously reported gas phase spectra, originated from Cl_3. The most probable carrier of the matrix spectrum is Cl_3^-.

NCl(*a*) has been proposed as an alternative energy carrier for use in chemically driven iodine laser systems. For the design and development of NCl(*a*)/I lasers, energy transfer rate constants need to be determined for NCl(*a*). Consequently, we have initiated studies of the quenching of NCl(*a*) by I_2. The first objective has been to assess the relative importance of the E-V transfer process

$$NCl(a)+I_2(X, v=0) \rightarrow NCl(X)+I_2(X, v>30)$$

Although quenching of NCl(*a*) by I_2 is rapid, preliminary results indicate that E-V transfer is not the dominant mechanism.

2. Quenching of I* by $O_2(X)$

Reaction 1 is exothermic by 0.8 kcal mol^{-1} (E/R=401.4 K) in the forward direction ($I(^2P_{1/2})$ is referred to as I* in the following). For the purpose of modeling COIL kinetics, rate constants for both the forward and backward transfer steps are needed. In practice, the rate constant for the reverse reaction (k_b) is most easily measured. It is known that the quenching of I* by $O_2(X)$ is dominated by the E-E energy transfer process. Hence, measurements of the quenching rate constant yield good estimates for k_b. Once k_b is known, the forward rate constant (k_f) can be calculated reliably from the theoretical expression for the equilibrium constant. Rate constants for forward and backward transfer at room temperature are well-established. However, for supersonic COIL devices, knowledge of the temperature dependence of the rate constants over the range $150 \leq T \leq 300$ K is needed. As part of the effort to obtain this data, we have studied the quenching I* by O_2 at 150 K.

2A. Measurement of the rate constant for $I^*+O_2(X) \rightarrow I+O_2(a)$ at 150K in a two-dimensional Laval nozzle.

In the first series of experiments we used a two-dimensional Laval nozzle to generate low temperature gas flows. The nozzle was designed by Dr. David Plummer of Logicon RDA. This work is described in detail in reference 1. The results obtained at 150 K were not in agreement with a previous determination of k_b at 180 K[8], or the predictions of empirical equations used in computer models of COIL devices[1]. Our measurements yielded backward and forward rate constants of $k_b(150)=(4.6\pm1.0)\times10^{-12}$ and $k_f(150)=(5.0\pm1.1)\times10^{-11}$ cm^3 s^{-1}, while the COIL model equations predicted substantially larger rate constants of $k_b(150)=14.1\times10^{-12}$ and $k_f(150)=15.7\times10^{-11}$ cm^3 s^{-1}.

The COIL equations were derived from the experimental work of Deakin and Husain[8], who had made the only other low temperature measurements for k_b. We identified a possible reason why their rate constants may have been subject to a systematic error[1]. However, we also recognized the limitations of our own measurements. Our rate constant was determined from time-resolved observations of I* fluorescence in the presence of O_2. The properties of the two-dimensional Laval nozzle[1,9] used in these measurements imposed limitations on the time during which the fluorescence decay could be observed. A relatively slow IR detector was used, so the time limitation effectively resulted in an instrumental distortion problem (initially, a faster detector of adequate sensitivity was not available). Consequently, deconvolution of the I* signal was an essential component of the data analysis. The reliability of the deconvolution procedure

seemed reasonable but, given the disagreement with the accepted rate constants, additional confirmation that this did not introduce systematic errors was needed.

The $I^*+O_2(X)$ quenching measurements at 150 K have since been repeated using a fast IR detector. For these experiments, an intrinsic Ge device with a response time of 1 μs was obtained on loan from the Applied Detector Corporation. This instrument permitted direct measurement of undistorted fluorescence decay curves within the time limits imposed by the two-dimensional Laval nozzle. The decay rate was determined as a function of the O_2 pressure. The results are shown graphically in Fig. 1. A linear fit to these data yielded a rate constant of $k_b(150)=(4.4\pm1.5)\times10^{-12}$ cm^3 s^{-1}, in good agreement with the value obtained using the slow detector. Note that the data from the fast detector were more scattered due to the lower sensitivity of this device (for comparison, see Fig.4 of reference 1).

2B. Detection of I by laser induced fluorescence (LIF) and measurement of the $I^*+O_2(X)$ quenching rate constant using LIF detection.*

As an alternative means for observing I* populations with good time resolution, we examined the possibility of using LIF as a detection method. For many years the electronic transition $5p^4(^3P)6s$, $^2P_{3/2} \leftarrow 5p^5$, $^2P_{1/2}$ (206.2 nm) has been used to follow I* concentrations. This has been done using atomic resonance lamps in absorption or resonance fluorescence configurations. Now, with the ready availability of materials that can be used to generate tunable laser light at 206 nm, it is possible to detect I* by UV LIF. However, prior to the work reported here, such detection had not been reported. The potential advantages of I* LIF detection are that it can provide high sensitivity and fast response. In addition, by spreading the laser beam out into a sheet, imaging of the I* concentration in a flow field should be feasible (this would be analogous to the LIF imaging of OH concentrations in flames).

For initial demonstration purposes, I* was generated by pulsed photolysis of I_2 at 498 nm. A frequency-doubled tunable pulsed laser was used to excite the I*. Fig. 2 shows a scan over the atomic lines. Note that the transition is structured due to hyperfine splitting of the lower level. The F"=2 and F"=3 components are split by 0.66 cm^{-1}. This splitting is partially resolved in Fig. 2, which was recorded using a laser linewidth of 0.4 cm^{-1}. Hyperfine interactions split the upper level into four components (F'=1, 2, 3, and 4), but these splitting were too small to be resolved in our measurements. It is clear from Fig. 2 that even low resolution LIF measurements can be used to monitor populations in specific I* hyperfine levels.

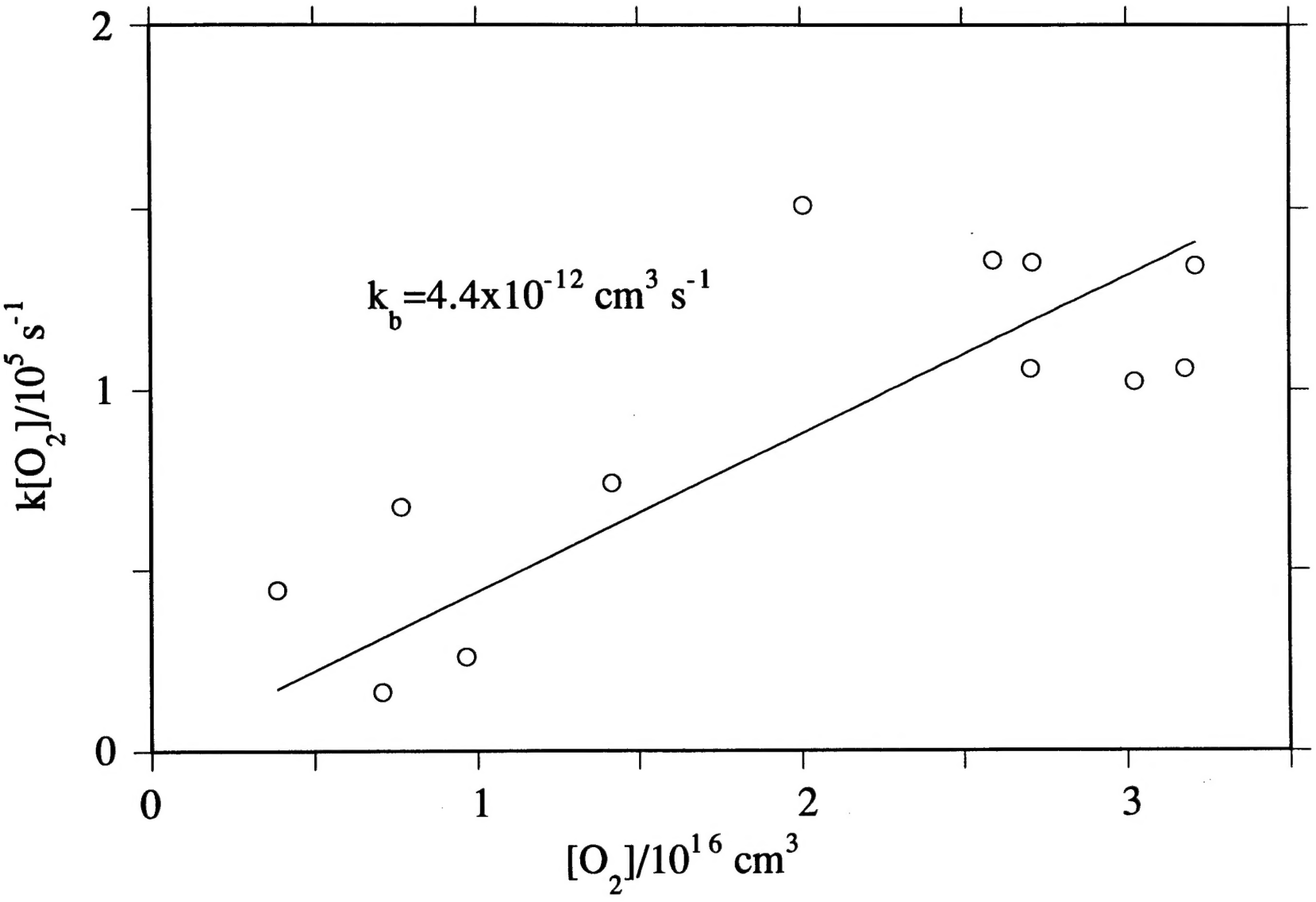

Figure 1. Quenching of I* by O_2 at 150 K. Data taken using a fast IR detector.

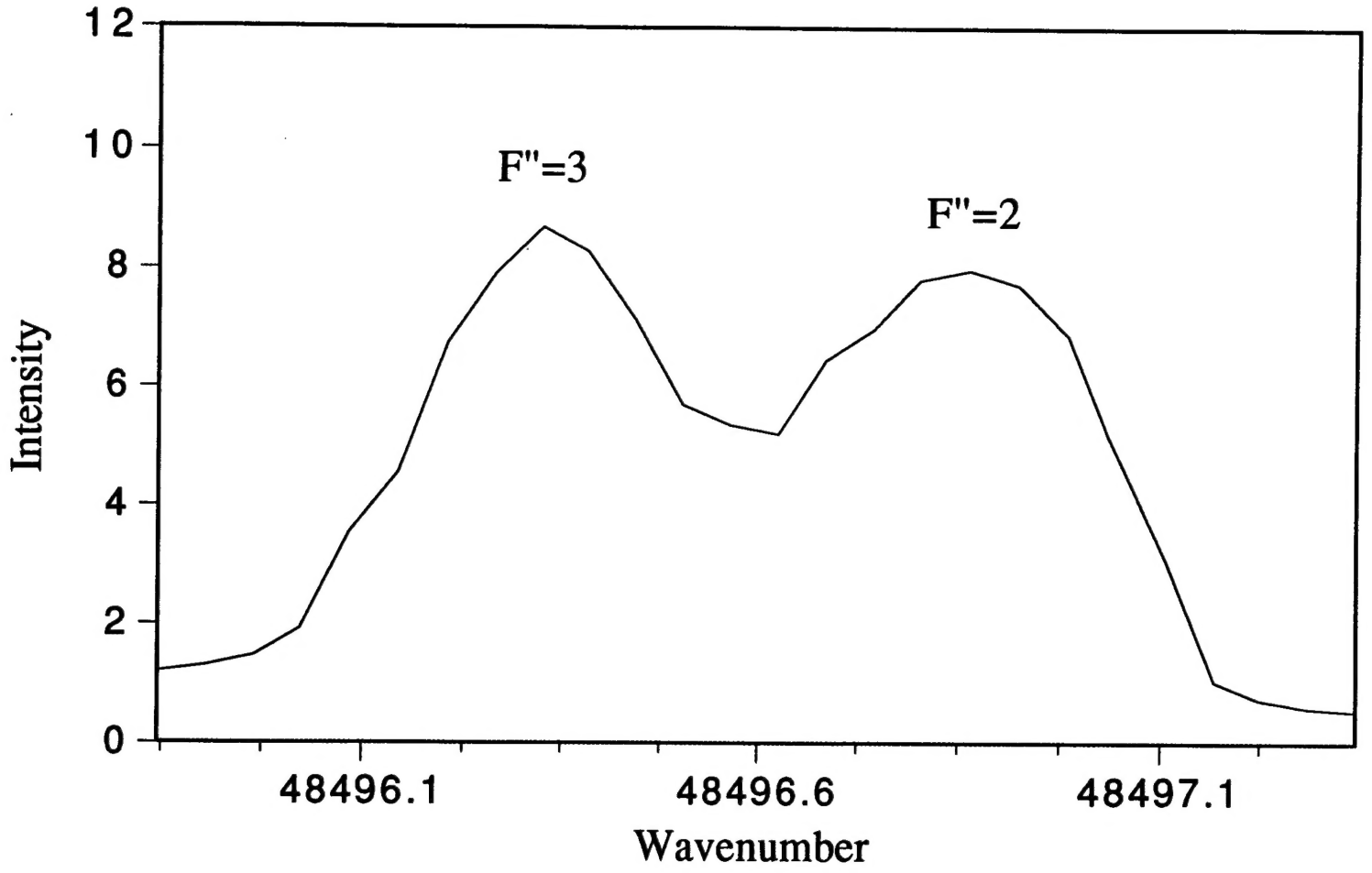

Figure 2. LIF scan of the I $5p^4 6s\ (^2P_{3/2})$ - $5p^5\ (^2P_{1/2})$ transition.

Having demonstrated LIF detection of I*, we then used this technique to measure the I* + O_2 quenching rate constant in the Laval nozzle. The photolysis and probe laser beams were positioned to cross the flow in the Laval nozzle, with the probe laser positioned about 5 mm downstream from the photolysis laser. The I* concentration was monitored with a fixed time delay between the photolysis and probe pulses. The relative I* concentration was recorded as a function of added O_2. For the conditions of this experiment, the I* concentration could be represented by the equation

$$[I^*] = [I^*]_0 e^{-(\Gamma + k_b[O_2])t} \tag{1}$$

where $[I^*]_0$ is the initial I* concentration, and Γ includes the effects of quenching by residual I_2 and collisions with the walls. To extract k_b from the relative [I*] measurements, Eq. (1) was expressed in the form

$$-\ln\left(\frac{[I^*]}{[I^*]_0}\right) = (\Gamma + k_b[O_2])t \tag{2}$$

(note that t was defined by the delay between the laser pulses). Fig. 3 shows the experimental data plotted in against the axes suggested by Eq. (2). A linear fit to these data yielded a quenching rate constant of $k_b(150)=(7.6\pm1.0)\times10^{-12}$ cm^3 s^{-1}. This value was about 1.7 times greater than that obtained from the IR fluorescence measurements, but still a factor of two smaller than the prediction of the COIL model equation[1]. Despite the large error bounds on the rate constants determined by IR fluorescence and I* LIF, their error ranges did not overlap. The reason for this discrepancy was not firmly established, but it is likely that the LIF measurements were subject to a systematic error. Adding O_2 to the He/I_2 flow in the nozzle reduced the velocity of the flow. However, the delay for I* detection was optimized with no added O_2, and the delay and laser positions were kept fixed throughout the measurements. As O_2 was added the loss of I* reflected both quenching and the timing error introduced by the concomitant change in the flow velocity. The latter would, of course, result in an overestimation of the quenching rate constant. It would have been a straightforward matter to verify the presence of this systematic error, had all of the equipment used for the measurements been available for sufficient time. However, the BBO doubling crystal used to generate 206 nm pulse was obtained on short-term loan from Lambda Physik, and was only available for one set of experiments. By the time we had analyzed the data and discovered the possible error, the crystal had been recalled by Lambda Physik.

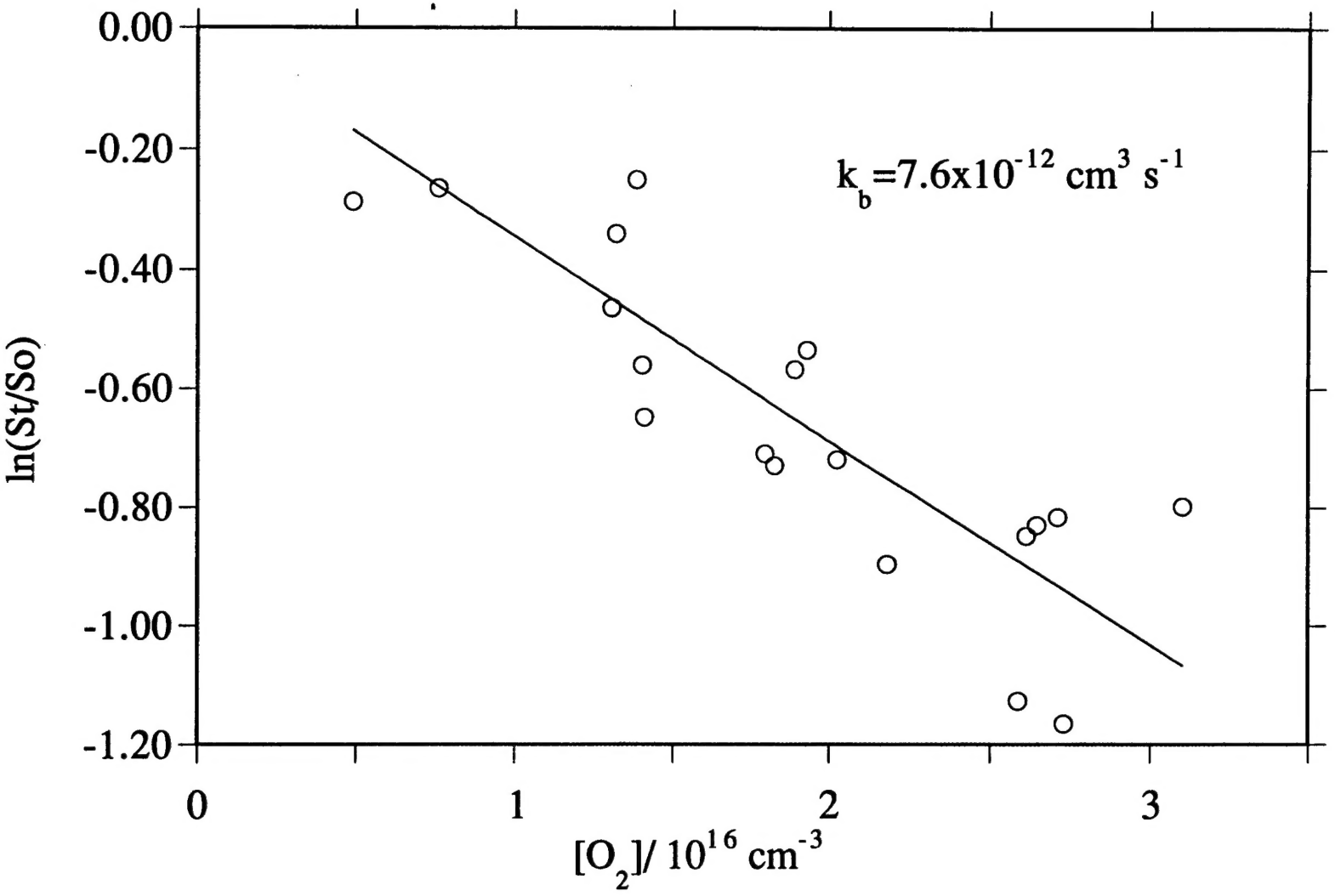

Figure 3. Stern-Volmer plot for quenching of I* by O_2 at 150 K.
These data were recorded using LIF detection of I*

2C. Measurement of the rate constant for $I^*+O_2(X) \rightarrow I+O_2(a)$ at 165K in an axis symmetric Laval nozzle.

Two significant problems were encountered in using the two-dimensional Laval nozzle[1]. Both were related to the requirement that measurements be made inside the body of the nozzle. The first problem, as noted above, was that fast transit through the constant pressure region limited the observation time. The second problem came from the severe scattering of laser light by the nozzle side windows (see Fig. 1 of reference 1). These problems can be mitigated by using axis symmetric Laval nozzles[9]. Consequently, we are continuing our studies of reaction [1] using these devices. In collaboration with Dr. David Plummer, we designed nozzles that span the temperature range from 125 to 200 K. For initial tests, the unit designed for operation at 170 K (Mach 1.5) was fabricated by the machine shop at Emory. The performance of this nozzle was evaluated by using I_2 fluorescence as a non-intrusive probe of local conditions. Flow field visualization was achieved by using a tunable CW laser to excite I_2 fluorescence. From these measurements it could be seen that a collimated supersonic gas flow was sustained by the nozzle. The local conditions within this flow appeared to be constant over a distance extending at least 4 cm from the nozzle exit plane. Rotationally resolved I_2 B-X spectra, recorded from the central region of the supersonic flow, were consistent with a local temperature of 165±10 K.

I^*+O_2 quenching measurements were made by observing time-resolved I^* fluorescence in the flow emanating from the axis symmetric nozzle. A Stern-Volmer plot derived from these measurements is shown in Fig. 4. This plot defined a quenching rate constant of $(5.2\pm0.4)\times10^{-12}$ cm^3 s^{-1}, in good agreement with the value obtained at 150 K in the 2-D nozzle.

2D. Theoretical analysis of the temperature dependence of the $I^* + O_2(X)$ quenching rate constant: Ab initio electronic structure calculations for the $I + O_2$ system.

In their study of the effect of temperature on the I^*+O_2 quenching rate constant, Deakin and Husain[2] examined the fit of their data for $k_b(T)$ to the standard Arrhenius expression

$$k_b(T) = Ae^{-E_{act}/RT} \qquad (3)$$

They obtained an activation energy (E_{act}) that was less than the endothermicity of the transfer event. To remedy this obvious anomaly, they proposed that the pre-exponential factor (A) was inversely dependent on temperature. On the basis of this suggestion, the equations for $k_b(T)$ and $k_f(T)$ currently used in COIL models assume that E_{act} is equal to the

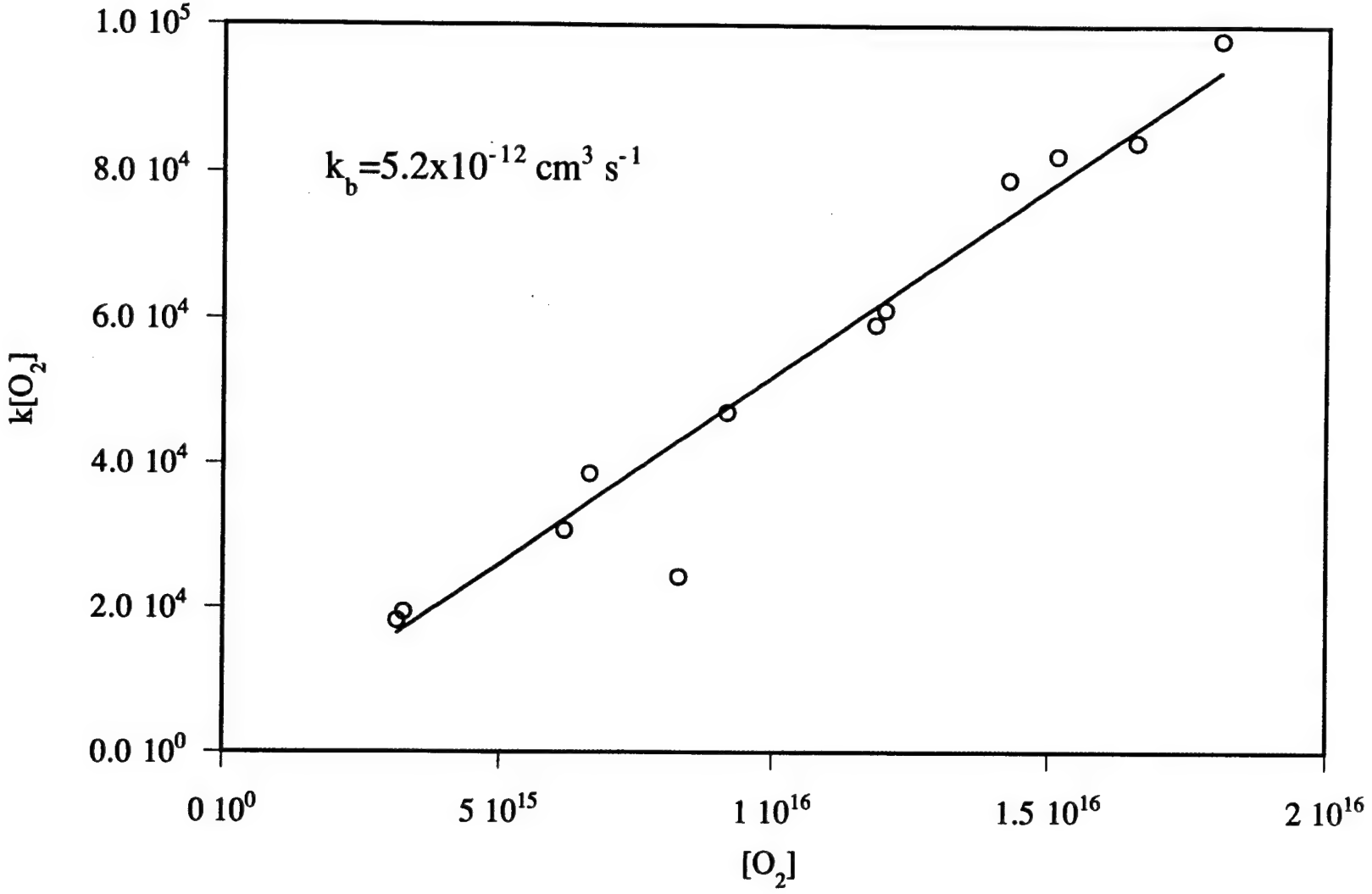

Figure 4. Stern-Volmer plot for quenching of I* by O_2 at 165 K
Data taken using the axis-symmetric Laval nozzle.

endothermicity of the transfer, and that $A=\sigma/T$. An equation for $k_f(T)$ that is inversely proportional to temperature implies that the collision dynamics are influenced by long-range attractive forces (and possibly transient formation of a long-lived collision complex).

The present results for k_b at temperatures below 180 K, when combined with room temperature data, lead to different conclusions. If we assume that the rate constants obtained from the IR fluorescence measurements are correct, the data can be represented by the expression

$$k_b(T) = \sigma\langle v\rangle e^{-E_{act}/RT} \tag{4}$$

where σ is a temperature independent transfer cross section and $\langle v\rangle$ is the average speed ($\propto T^{1/2}$). If the LIF measurement is assumed to be correct, the data give a good fit to Eq. 3. Agreement with Eq.'s 3 or 4 implies that, i) long-range attractive forces are not important in the collision dynamics and, ii) transfer is mediated by surface intersections (in a diabatic representation) that occur near or below the $O_2(a)$ + I dissociation asymptote.

To gain a deeper understanding of the $I(^2P_{3/2}) + O_2(a) \leftrightarrow I(^2P_{1/2}) + O_2(X)$ system we performed high-level *ab initio* calculations to predict the potential energy surfaces of states that correlate with the $I(^2P_{3/2}) + O_2(a)$ and $I(^2P_{1/2}) + O_2(X)$ dissociation limits (work done in collaboration with Prof. K. Morokuma). Given the above considerations, we were particularly interested to know if there are any deeply bound states that correlate with $I(^2P_{3/2}) + O_2(a)$, and the energy regions where the diabatic surfaces from the two dissociation limits intersect. *Ab initio* calculations were performed using the MOLPRO96 package of programs. For oxygen, Dunning's au-cc-valence triple zeta (VTZ) polarized basis set was used. The iodine basis set consisted of Dolg et al.'s[10] relativistic effective core potential plus polarized VTZ. CASPT2 and CASSCF levels of theory were used. The spin-orbit interaction was calculated perturbationally using CASSCF wavefunctions to diagonalize the one-electron Breit-Pauli operator

$$\hat{H}_{SO} \cong \frac{\alpha^2}{2}\sum_a\sum_i Z_{eff}\frac{\mathbf{r}_{ia}\times\mathbf{p}_i}{|\mathbf{r}_{ia}|^3}\cdot\sigma_i \tag{5}$$

(the program GAMESS96 was used for this step). As the O_2 bond length is quite similar in the X and a states, calculations were performed with r_{O_2} fixed at the $\langle X, v=0|r|a, v=0\rangle/\langle X, v=0|a, v=0\rangle$ centroid.

Spin-coupled calculations revealed crossing seams between potential energy surfaces arising from the $I(^2P_{3/2})+O_2(a)$ and $I(^2P_{1/2})+O_2(X)$ asymptotes. Radial cuts through the potential surfaces were calculated for several different angles. These cuts showed their deepest minima and lowest energy curve crossings for angles around 50°.

Fig. 5 shows diabatic cuts for θ=50°. Note that the states are bound by 250 cm^{-1} or less, indicative of weak dispersive interactions. There are several curve crossings that occur below the $O_2(a)$+I dissociation limit. This supports the notion that electronic energy transfer between I and O_2 is mediated by surface intersections, and that quenching of $I(^2P_{1/2})$ by $O_2(X)$ should be characterized by an activation energy of $E_{act} = \Delta U = 279\ cm^{-1}$. The attractive forces acting between $I(^2P_{3/2})+O_2(a)$ are too weak be of importance in determining the exothermic transfer rate constant (k_f) over the temperature range of interest (T>100K). Owing to the relatively strong mixings of the diabatic states, the Landau-Zener model is not suitable for developing an estimate for k_f from the potentials. However, a rough value for k_f can be obtained by considering the curves shown in Fig. 5. The avoided crossings occur in the R=6.5-7 au range, so we assume that collisions with impact parameters of b≤6.5 au may result in transfer. As only two of the four states that correlate with $I(^2P_{3/2})+O_2(a)$ are crossed by lower states, only half of the collisions will occur on suitable surfaces. We further assume that collisions that traverse the crossing region sample the states statistically. As two upper surfaces are crossed by three lower surfaces, this yields a probability of 3/5 for exit on one of the lower surfaces. These considerations lead to a transfer cross section of $\sigma_f = \frac{1}{2}\cdot\frac{3}{5}\pi b_{max}^2 = 40\ au^2$. Taken with the average collision velocity, this yields a 295 K rate constant of $k_f = 5.5\times10^{-11}\ cm^3\ s^{-1}$. Given the severity of the approximations, this is in reasonable agreement with the experimental value of $(7.8\pm0.6)\times10^{-11}\ cm^3\ s^{-1}$.

The primary conclusion drawn from the *ab initio* study is that potential energy surfaces for $I(^2P_{3/2})+O_2(a)$ and $I(^2P_{1/2})+O_2(X)$ are not consistent with the previous hypothesis that $k_f \propto T^{-1}$. The surfaces are in accord with the low temperature I^*+O_2 quenching rate constants presented here, and the above suggestion that the $O_2(a)$+I transfer cross section is approximately constant over the range 150<T<300 K.

3. Collisional relaxation of highly excited vibrational levels of $I_2(X)$.

3A. Rate constants measured at room temperature

Rotational and vibrational energy transfer rate constants were measured for excited ro-vibrational levels of $I_2(X)$. SEP was used to excite the levels v=23, J=57 and v=38, J=49 via the *B-X* transition. LIF from the *D-X* system was used to follow the collision dynamics. Energy transfer processes induced by collisions with He, Ar, N_2, O_2, Cl_2, I_2 and H_2O were investigated. The results, combined with re-analyzed data from earlier SEP/LIF measurements, provide an overview of the collision dynamics of $I_2^{\dagger}$ levels in the

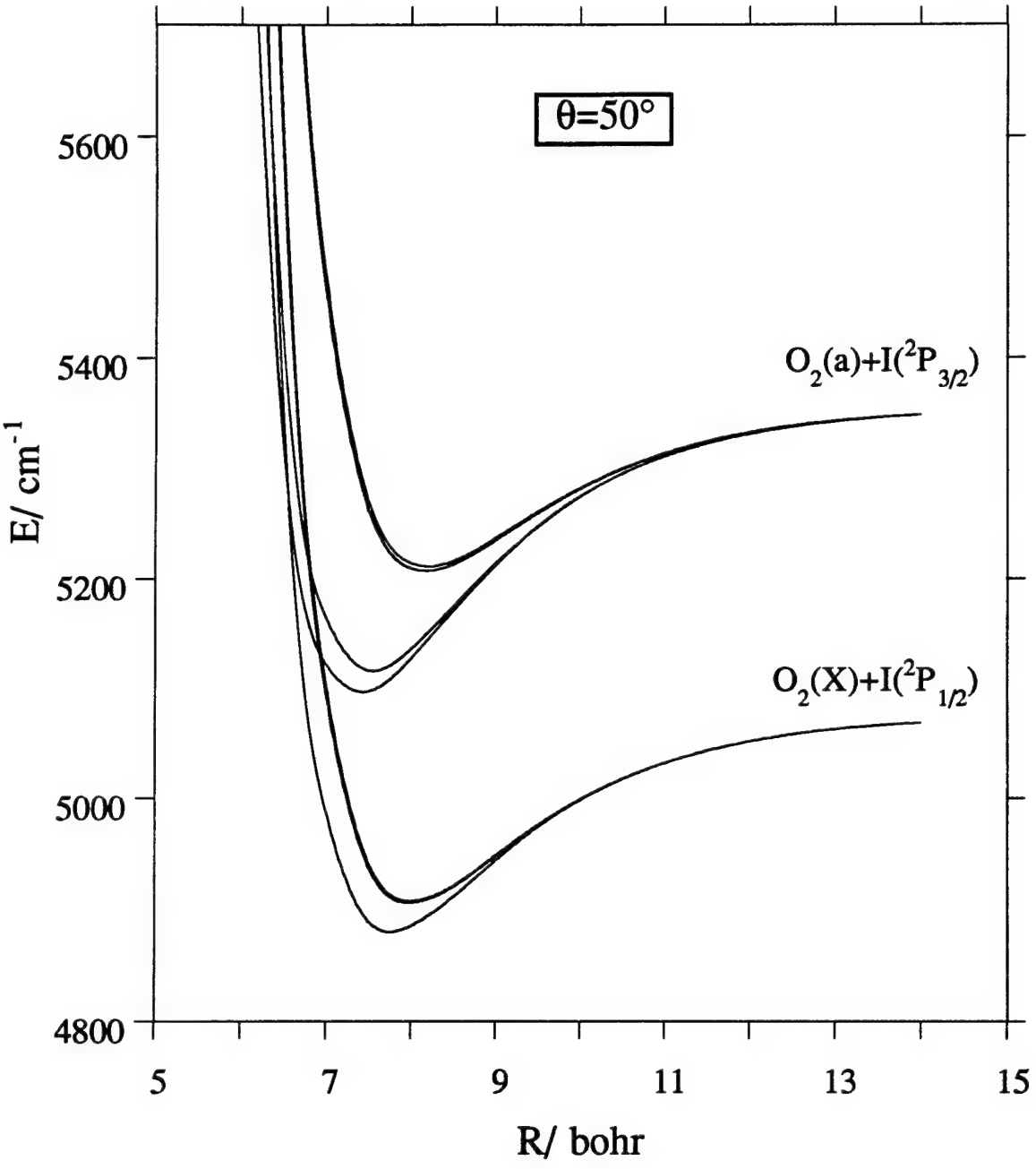

Figure 5. Ab initio potential energy curves for IO_2

range $23 \le v \le 42$[2,3]. It appears that the behavior of these levels can be reasonably well represented by classical models. For all of the collision partners examined, rotationally inelastic collisions dominated. The probability for angular momentum transfer was proportional to the collision momentum for non-polar collision partners. The distributions of final rotational levels populated by collisions could be adequately modeled using either the statistical energy gap or energy corrected sudden scaling laws. The data were not accurate enough to assess the relative suitability of these two models. Rotational energy transfer parameters derived from the models were not sensitive to the initial vibrational level.

Comparisons of the *X* and *B* state rotational energy transfer dynamics indicate that the two states behave similarly with collision partners that do not induce significant electronic state mixings. Thus, the adoption of *B* state rotational transfer parameters for ground state levels should be a viable approximation for colliders that are poor quenchers, provided that the *B* and *X* state levels have similar rotational constants. For species that are good *B* state quenchers, it appears that the rotational energy transfer probabilities are diminished, relative to the *X* state, by the competition with electronic energy transfer. However, the data obtained so far suggest that the distributions of final rotational states populated by collisions with good quenchers are not strongly influenced by electronic effects. Model parameters that reflect the probabilities for transferring specific amounts of angular momentum are not much different for equivalent levels of the *B* and *X* states, even for efficient quenching agents.

The characteristics of $I_2^{\dagger}$ vibrational energy transfer were in qualitative agreement with results from classical trajectory calculations. Vibrational and rotational energy transfer are not strongly coupled, and the rotational distributions resulting from $\Delta v=0$ and $\Delta v=-1$ events were similar. The probabilities for vibrational energy transfer were approximately proportional to the collision momentum for all collision partners, with the exception of I_2. All of these properties of the ground state collision dynamics have been noted previously for $I_2(B)$.

Effective rate constants for the collisional deactivation of $I_2^{\dagger}$ are needed for computer models of COIL systems. A kinetic model was developed to determine the deactivation rate constants ($k_M^{\dagger}$) from the state-to-state transfer rate constants. The results for O_2 ($k_{O_2}^{\dagger}=6\times10^{-12}$ cm^3 s^{-1})[3] and H_2O ($k_{H_2O}^{\dagger}=1.3\times10^{-11}$ cm^3 s^{-1})[3] were in disagreement with the assumed rate constants currently in use (5×10^{-11} and 3×10^{-10} cm^3 s^{-1}, respectively)[11]. For He, the effective rate constant from the present work ($k_{He}^{\dagger}=8\times10^{-12}$ cm^3 s^{-1}) was a factor of two greater that the estimate used in earlier models[11], but a factor

of six smaller than the value derived from a model of a high pressure COIL device[12]. The latter discrepancy is probably a consequence of other errors in the standard rate constant set.

3B Rate constants measured at temperatures near 10K

Vibrational relaxation of $I_2^{\dagger}$ induced by low energy collisions was investigated in free-jet expansions driven by He or Ar. These measurements were performed by focusing state preparation and probe laser beams into the downstream region of He or Ar expansions that had been seeded with I_2. Transfer out of the initial vibrational levels v"=23 and v=42 was examined in the temperature range 3-15 K. For these conditions the probe laser spectra are quite simple and uncongested. Due to the small number of rotational levels that are thermally populated in the expansion, coupled with the fact that vibrational energy transfer is not accompanied by large changes in the angular momentum, the vibronic bands do not overlap. Consequently, relative vibrational populations can be assessed from the areas of unresolved rotational band contours. In addition to knowing the relative populations at given delay times, the local temperature and gas density in the expansion must be known for determinations of the transfer rate constants. These properties were obtained from the thermodynamic relationship

$$\frac{\rho}{\rho_0} = \left(\frac{T}{T_0}\right)^{3/2} = 0.16\left(\frac{x}{D}\right)^{-2}$$

where ρ is the local gas density (cm^{-3}), T is the local temperature, x is the distance from the nozzle orifice, and D is the nozzle diameter (0.8 mm for the results reported here). ρ_0 and T_0 are the density and temperature of the gas prior to expansion, which are easily measured quantities. This equation was used to determine ρ and T from measurements of the separation between the nozzle orifice and the laser beams.

Probe laser spectra for collisions with He, recorded after a delay that permitted several collisions, showed populations in levels corresponding to Δv=-1, -2, and -3. Similar spectra for I_2 in an Ar expansion showed mostly Δv=-1 transfer, with very small populations in the Δv=-2 levels. These data were analyzed by fitting the time-dependent relative vibrational populations to a kinetic model defined by the rate equations

$$\frac{d[v]}{dt} = \sum_{v'}(-k_{v-v'}[v] + k_{v'-v}[v'])[M]$$

where [v] and [v'] are the relative populations in levels v and v', $k_{v-v'}$ is the rate constant for transfer from level v to level v', and [M] is the number density of the collider gas (He or Ar). This equation was solved by numerical integration, and the transfer rate constants

were obtained by least squares fitting to the relative populations. As the temperature was very low, only downward energy transfer was included in the model. Two different assumptions about the dependence of $k_{v-v'}$ on Δv (=v'-v) were examined. In the first model it was assumed that relaxation occurred by sequential Δv=-1 steps; the rate constants for single-collision multi-quantum jumps were set to zero. In the second model the transfer rate constants were represented by the expression

$$k_{v-v'} = k_{v-(v-1)} \exp(-\alpha(1- | \Delta v |))$$

which permits multi-quantum steps.

Vibrational transfer rate constants derived from the kinetic models are presented in Table 1. For collisions with He, the fit given by the multi-quantum jump model was clearly superior to that obtained using the single quantum jump model. Even so, the Δv=-1 process accounted for more than 75% of the total removal rate constant. For transfer out of v=23 the total removal rate constant was around 1.6×10^{-11} cm^3 s^{-1}. This was roughly an order of magnitude smaller than the He vibrational relaxation rate constant at room temperature (1.7×10^{-10} cm^3 s^{-1}). Part of this difference derives from the change in the collision frequency. To compensate for this factor, it is helpful to calculate effective vibrational relaxation cross sections from $\sigma_{v-v'} = k_{v-v'}/\langle v \rangle$, where $\langle v \rangle$ is the average relative speed of the collision partners. Effective cross sections for I_2 v"=23 + He are listed in Table 1. These values are comparable to the room temperature cross section of 9.5×10^{-15} cm^{-2}, which suggests that the cross section is insensitive to temperature. In one set of measurements, low temperature (3.3 K) data for I_2 v"=42 + He yielded transfer cross sections that were very close to the values obtained for v"=23. This was consistent with our room temperature results, where we had found that the vibrational transfer rate constant was not dependent on v" over the range 22<v"<43. A second set of measurements at 5 K yielded a lower cross section. We suspect that this second data set was subject to some systematic error, but we have not yet determined the source of the problem.

The Ar data set was analyzed using both the single and multiple quantum jump models. However, the best fit obtained with the multi-quantum model yielded a very large α value, indicating that transfer events with $| \Delta v | \geq 2$ were not significant. Vibrational transfer rate constants and cross sections for I_2+Ar are given in Table 1. In contrast to the situation for He, the cross section for Ar appears to be strongly dependent on the temperature. The values obtained at 13 K were nearly an order of magnitude smaller than the room temperature results. Furthermore, it appears that the cross section shows some dependence on the initial vibrational level.

Table 1

Vibrational Energy Transfer Rate Constants and Collision Cross Sections for $I_2(X)$ + Rg at Low Temperature

			Single Quantum Jump Model		Multiple Quantum Jump Model			
	Temp (K)	Backing Pressure (PSIA)	$k_{v \rightarrow v-1}$ ($x10^{-11}cm^3/s$)	Cross Section $Å^2$	α	$k_{v \rightarrow v-1}$ ($x10^{-11}cm^3/s$)	$k_{v \rightarrow v-1,v-2,v-3}$ ($x10^{-11}cm^3/s$)	Cross Section $Å^2$
Helium								
v=23	3.3	130	1.56 (0.30)	11.7 (2.2)	1.4 (0.4)	1.26 (0.34)	1.65 (0.40)	12.4 (3.0)
		155	1.61 (0.25)	12.1 (1.9)	1.5 (0.4)	1.33 (0.20)	1.70 (0.24)	12.8 (1.8)
	4.7	130	1.26 (0.35)	8.0 (2.2)	1.2 (0.3)	0.97 (0.22)	1.34 (0.28)	8.4 (1.8)
		155	1.26 (0.30)	8.0 (1.9)	1.3 (0.4)	0.97 (0.16)	1.30 (0.20)	8.2 (1.3)
	5.0	130	1.50 (0.35)	9.1 (2.1)	0.8 (0.4)	0.94 (0.25)	1.56 (0.30)	9.5 (1.8)
		155	1.56 (0.25)	9.5 (1.5)	0.8 (0.3)	0.94 (0.25)	1.56 (0.35)	9.5 (2.1)
v=42	3.3	130	1.13 (0.21)	8.5 (1.6)	1.1 (0.4)	0.88 (0.23)	1.27 (0.30)	9.5 (2.2)
		155	0.94 (0.30)	7.1 (2.3)	1.0 (0.3)	0.71 (0.20)	1.07 (0.30)	8.0 (2.2)
	5.0	130	0.73 (0.20)	4.5 (1.2)	1.0 (0.4)	0.55 (0.15)	0.82 (0.22)	5.0 (1.3)
		155	0.63 (0.20)	3.8 (1.2)	0.6 (0.4)	0.39 (0.15)	0.72 (0.26)	4.4 (1.6)
Argon								
v=23	13.1	30	0.098 (0.023)	1.1 (0.3)	------	------	------	------
v=42	13.1	35	0.23 (0.08)	2.6 (0.9)	------	------	------	------

1-σ Error limits are given in parentheses

The vibrational transfer cross sections for collisions with He or Ar did not provide evidence of enhancements resulting from the action of long-range forces and/or resonances. It is of interest to note that the results for Ar are consistent with the expectations of Landau-Teller theory, while the He data are in disagreement with these models. With regard to COIL systems, the most significant implication of these measurements is that vibrational relaxation of $I_2^{\dagger}$ by He proceeds with a cross section that is approximately independent of temperature and initial vibrational level.

4. Photolysis of matrix isolated $HX\text{-}X_2$ dimers.

For the reasons outlined in the introduction, we have investigated a method for trapping trihalogens in rare gas solids. Using standard co-deposition techniques, $HX\text{-}X_2$ dimers were trapped in solid Ar. The dimers were then photolyzed *in situ* by pulses from an ArF laser. The basic idea was that H atoms may be ejected from a matrix cage on photolysis, whereas the bulky and slow moving halogen atoms have very low probabilities for cage escape. The first tests of this method were carried out on $HCl\text{-}Cl_2$ dimers.

In-situ photolysis of Cl_2/HCl/Ar matrices generated a new species that was characterized through laser excitation and wavelength resolved fluorescence measurements[6]. After 193 nm photolysis, 308 nm excitation of the matrices produced a broad emission band centered at 470 nm. This band was emitted with a lifetime of 44 μs at a temperature of 12 K. An excitation spectrum obtained by monitoring the 470 nm emission exhibited a single broad peak centered at 312 nm. Control experiments demonstrated that the new species was not one of the transient species resulting from photolysis of HCl/Ar or Cl_2/Ar alone (e.g., Ar_2H^+ or HCl_2^-). The emission spectrum and lifetime were in agreement with gas phase results that were previously attributed to Cl_3[4,5]. The excitation spectrum correlated with the 320 nm absorption band of the isoelectronic F_2Cl radical. These elements of circumstantial evidence indicated that Cl_3 was the carrier of the 470 nm emission.

Previous investigators used results from *ab initio* calculations to support the assignment of their gas phase spectra to Cl_3[4,5]. To gain further insights we performed calculations using higher levels of theory, which explored more regions of the coordinate space. As described in the following section and reference 7, we found that the previous calculations were in error, and that neither the matrix or gas phase spectra could be assigned to Cl_3.

Subsequent investigations of the 470 nm emission band showed that the fluorescence decay lifetime was sensitively dependent on temperature (the lifetime decreased with increasing temperature, while the fluorescence quantum yield remained

constant). Measurements of the IR absorption spectrum showed that a negligible fraction of the HCl-Cl_2 complexes were permanently dissociated by 193 nm excitation. Nor was the free HCl in the matrix noticeably destroyed (the IR spectrometer used for these measurements was not available at the beginning of the project). We currently suspect that the carrier of the 470 nm band is Cl_3^-, produced in the disordered grain boundary regions of the matrix where escape of the H atoms (and H^+ ions) is possible. As the fraction of material trapped in the grain boundary regions was very small (<1%), the photolysis and photoionization events could not be detected by their IR signatures (or perceptible destruction of parent compounds)

193 nm photolysis of HBr releases more kinetic energy to the fragments than the corresponding dissociation of HCl. By monitoring the IR absorption of matrix isolated HBr we have demonstrated that 193 nm photolysis in Ar results in permanent cage escape of the H atom. Experiments involving the production of Br_3 via photolysis of HBr-Br_2 dimers are in progress.

5. *Ab initio* molecular orbital study of the tricholrine radical.

High-level *ab initio* calculations were performed to investigate the electronic structure of Cl_3 and predict the characteristics of its low-lying electronic transitions. This work, done in collaboration with Prof. K. Morokuma, is described in detail in reference 7. CASSCF, (IC)MRSDCI, CASPT2, CCSD levels of theory were used to explore the potential energy surfaces of the ground and excited electronic states with avdz and avtz basis sets. The ground state potential surface has two van der Waals minima, one corresponding to an asymmetric linear structure $\tilde{\mathbf{X}}\mathbf{L}$ ($\tilde{X}^2\Pi$), and the other to a bent structure $\tilde{\mathbf{X}}'\mathbf{B}$ ($\tilde{X}^2A'$). The bent symmetric structure $\mathbf{TS}\text{-}\tilde{\mathbf{X}}'\mathbf{V}$ ($\tilde{X}^2A_1$) is a transition state for exchange of a chlorine atom between van der Waals complexes. Of the excited doublet states a linear symmetric structure $\mathbf{2L}(1^2\Pi_g)$ with r_1 = 4.67 bohr was the only strongly bound state, located about 8,700 cm^{-1} above the global minimum $\tilde{\mathbf{X}}\mathbf{L}$. Two bound quartet states were found. The most deeply bound quartet state, $1^4A_1'$, had a D_{3h} geometry at the minimum (**QD3h**; r=5.0 bohr), which was about 11,300 cm^{-1} above $\tilde{\mathbf{X}}\mathbf{L}$. The 1^4A_2 state had a minimum for a C_{2v} geometry (**QC2v**; r_1 = 5.12 bohr and θ = 100.5°) lying about 13,500 cm^{-1} above $\tilde{\mathbf{X}}\mathbf{L}$.

Kawasaki *et al*[4]. used results from an unpublished *ab initio* calculation to assign their gas phase spectrum to Cl_3. This calculation predicted absorption transitions at 680

and 370 nm. The transitions were assigned to $1^2B_2 \leftarrow \tilde{X}^2A_1$ and $2^2B_2 \leftarrow \tilde{X}^2A_1$, and the gas phase spectrum was attributed to the latter. The present calculations predict that vertical $1^2B_2 \leftarrow \tilde{X}^2A_1$ and $2^2B_2 \leftarrow \tilde{X}^2A_1$ transitions will occur near 730 nm and 450 nm, respectively. The 2^2B_2 state does not have bound regions, and will not emit to any significant degree. It is conceivable that the $2^2\Pi$-$\tilde{X}^2A'$ transition, originating from the van der Waals ground state, could be responsible for the absorption band detected by Kawasaki *et al*[4]. However, the emission characteristics of this system would not be consistent with their observations. The transition dipole is relatively small for the van der Waals geometry, where the transition is approximately $Cl_2(B^3\Pi)$-Cl $\leftarrow$ $Cl_2(X)$-Cl, but the transition dipole becomes large in the vicinity of the $2^2\Pi$ ($1^2\Pi_g$) state minimum. Hence, most transitions would occur in this coordinate region where the Franck-Condon factors will favor strong emission near 2 mm. The magnitude of the transition dipole would result in a lifetime of the order of 100 ns.

Bound quartet states that correlate with the $3Cl(^2P)$ dissociation limit were found in this study, but these cannot account for the gas phase or matrix spectra. Transitions to the bound regions of the quartet surfaces cannot occur at wavelengths shorter than 490 nm (predicated by a ground state well-depth of less than 600 cm^{-1}). Lastly, transitions to and from the ion-pair states cannot account for the gas phase or matrix spectra. Starting from $\tilde{X}$**L** or $\tilde{X}$**'B**, vertical transitions to the ion-pair states (or states with a significant fraction of ion-pair character) will occur at wavelengths shorter than 250 nm (the absorption in the matrix was centered at 312 nm). Emission from the ion-pair states could occur in the 400-500 nm range, but the large transition dipoles would result in short radiative lifetimes (<100 ns).

Thus, we conclude that it is most unlikely that any of the spectra that have been attributed to Cl_3 actually originate from this species.

6. NCl(*a*) + I and NCl(*a*) + I_2 energy transfer

NCl(*a*) has been identified as a promising energy transport agent for use in chemically driven iodine lasers. To further asses the potential of NCl for this application, we are studying transfer of electronic energy from NCl(*a*) to I_2 and I.

Our initial experiments were designed for qualitative investigation of the process

$$NCl(a) + I_2 \rightarrow NCl(X) + I_2$$

By analogy with the $O_2(a)$+I_2 system, it was anticipated that vibrationally excited I_2 would result from energy transfer. Hence, the intention was to generate NCl(*a*) in the presence of I_2, and search for $I_2^\dagger$ using the *D*-*X* transition for LIF detection. However, the source of

NCl(a) used in these experiments presented complications. The metastables were produced by pulsed 248 nm photolysis of N_3Cl, which yields kinetically hot NCl(a) and a small amount of NCl(b). The photolysis light could also weakly excite I_2. Under these conditions, the metastable A and A' states of I_2 could be populated by collisional energy transfer. Populations in the high vibrational levels of the ground state, and the low vibrational levels of the A and A' states could all be detected with high sensitivity using near-UV LIF. This poses a problem if all three states are populated, as the spectra become exceedingly congested and difficult to assign. Some separation of the band systems could be achieved by using a monochromator for wavelength-selected fluorescence detection. The D-X system has a long wavelength cut-off just beyond 320 nm, whereas the D'-A' and β-A systems have their strongest emissions near 340 nm. LIF spectra recorded with detection of 320 nm fluorescence will show bands of the D-X, β–A, and D'-A' systems. Spectra recorded with 340 nm detection will not show the D-X bands. Therefore, comparisons of spectra detected at the two different wavelengths provide a means for unambiguous identification of the D-X features. To further mitigate spectral congestion problems, experiments were performed in a supersonic expansion.

Premixed samples of N_3Cl and I_2 in He were photolyzed in the early stages of the expansion. Detection of the NCl b-X emission was used to verify that we were making adequate concentrations of N_3Cl. Fig. 6 shows an LIF spectrum for the I_2 states that were populated by primary and secondary photochemical events in the expansion. The populations in the A and A' states were not dependent on the presence of NCl in the expansion. These states were accessed by the processes

$$I_2(X) + h\upsilon_1(248\ nm) \rightarrow I_2(D)$$

$$I_2(D) + M \rightarrow I_2(\beta/D') + M$$

$$I_2(\beta/D') \rightarrow I_2(A/A') + h\upsilon_2$$

where M=He, Cl_2, or I_2. Although the I_2 D-X absorption is very weak at 248 nm, the powers needed to dissociate a significant fraction of the N_3Cl were also sufficient to excite the I_2.

Fig. 7 shows I_2 LIF spectra recorded in the presence of NCl(a). Comparison of the traces recorded with detection of 320 and 340 nm light clearly indicate population in a high vibrational level of $I_2^{\dagger}$. Through time-resolved measurements it was verified that $I_2^{\dagger}$ was excited by a mechanism that involved collisional energy transfer from NCl(a). However, from time-dependent studies of the I* in the system, and from approximate information about the range of $I_2^{\dagger}$ levels excited, it seems likely that $I_2^{\dagger}$ was excited by indirect processes. LIF of the 206.2 nm atomic transition was used to follow I* concentrations.

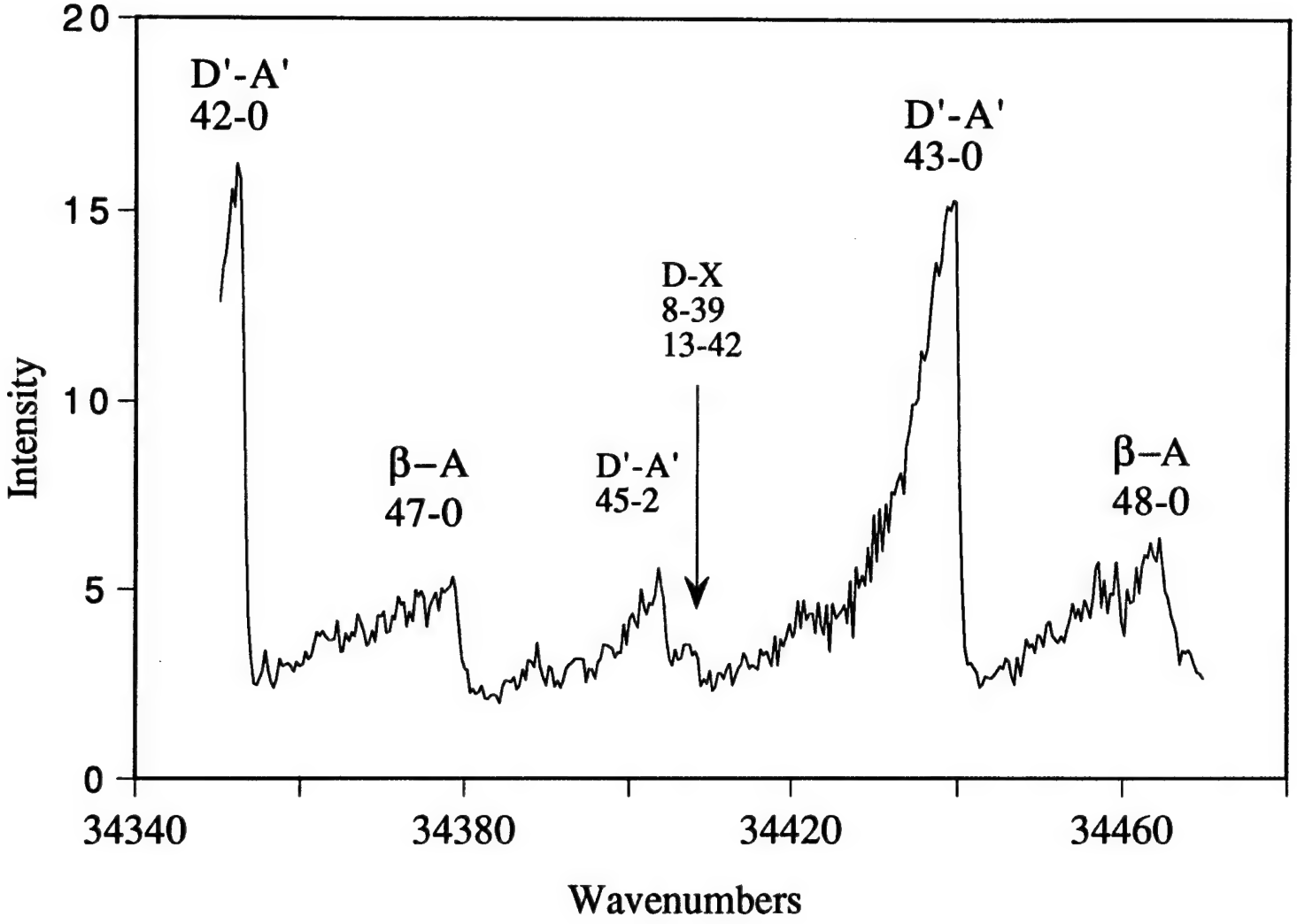

Figure 6. LIF spectrum of excited I_2 states resulting from 248 nm photolysis of an $He/N_3Cl/I_2$ mixture. This spectrum was detected by monitoring the fluorescence at 320 nm.

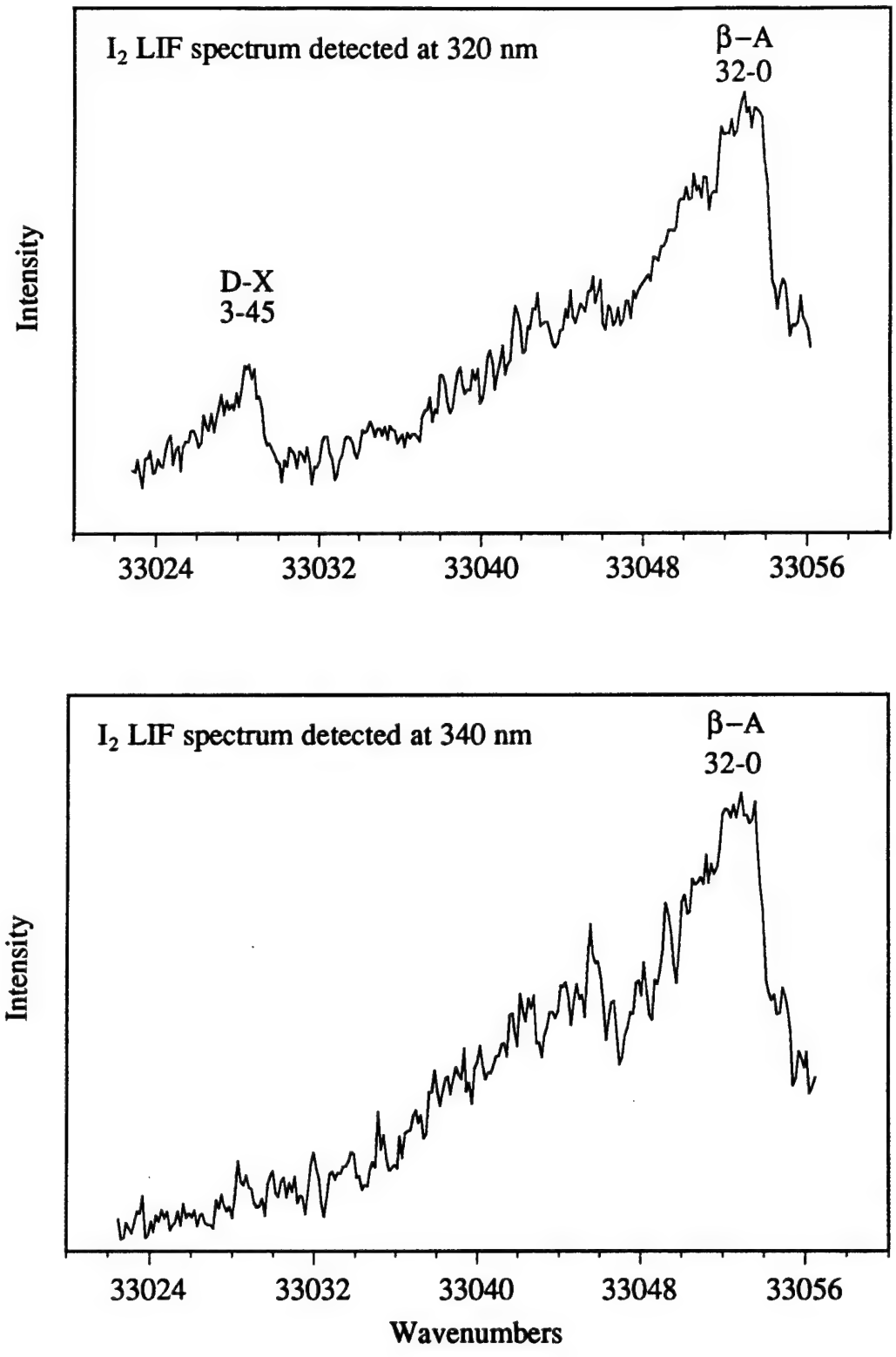

Figure 7. I_2 LIF spectra of states populated after photolysis of an N_3Cl/I_2/He mixture. Comparison of these traces provides a clear indication of the band arising from vibrationally excited $I_2(X)$

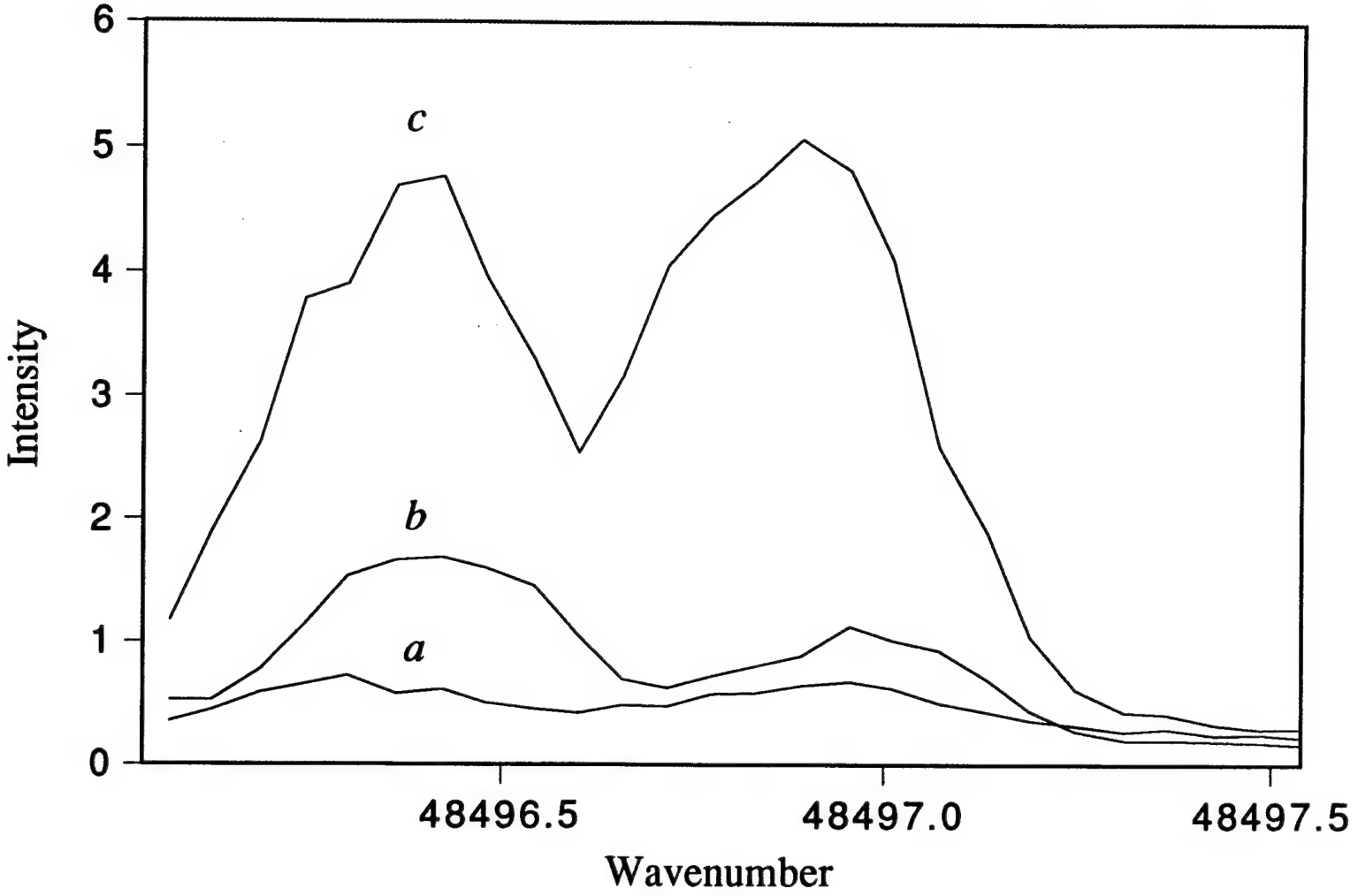

Figure 8. I* LIF signals following 248 nm photolysis of (a) I_2/He, (b) I_2/Cl_2/He, and (c) I_2/N_3Cl/He. See text for details.

Fig. 8 shows scans over the atomic line for three different conditions. Trace (a) was obtained after 248 nm photolysis of an He/I_2 expansion with no added Cl_2 or N_3Cl. A weak I* signal was detected, indicating the presence of a minor direct dissociation process

$$I_2(X) + h\upsilon_1(248\ nm) \rightarrow I + I^* \ (or\ 2I^*)$$

Trace (b) shows the effects of adding Cl_2 to the He/I_2 flow (these measurements were made because it is likely that some Cl_2 accompanies the N_3Cl). The presence of Cl_2 increased the I* signal. The most probable explanation is that some ICl was formed in the metal tubing prior to expansion. ICl readily yields I* on 248 nm photolysis. For both the He/I_2 and He/I_2/Cl_2 mixtures, experiments where the delay between the photolysis and probe laser pulses was varied gave results that were consistent with direct dissociation processes; the I* signals simply decayed with increasing delay time.

Trace (c) in Fig. 8 shows the I* signal resulting from photolysis of an He/I_2/N_3Cl mixture, which yielded the highest I* concentration. Time-resolved measurements revealed growth kinetics that were consistent with I* formation by collisional processes. This result could be interpreted in terms of a mechanism that involves dissociation of I_2 by NCl(a):

$$I_2(X) + NCl(a) \rightarrow I_2^\dagger + NCl(X)$$

$$I_2^\dagger + NCl(a) \rightarrow 2I + NCl(X)$$

$$I + NCl(a) \rightarrow I^* + NCl(X)$$

Alternatively, the I* could originate from transfer to the atomic I generated by I_2 photolysis:

$$I_2(X) + h\upsilon_1(248\ nm) \rightarrow I + I^* \ (and\ I{+}I)$$

$$I + NCl(a) \rightarrow I^* + NCl(X)$$

Note that $I_2^\dagger$ could be formed in this scheme by the very efficient E-V transfer process I* + $I_2(X) \rightarrow I_2^\dagger + I$. From the data obtained to date, it appears that the latter mechanism dominates. Transfer from NCl(a) to I_2 is expected to produce a vibrational population distribution with a maximum near v=50, while transfer from I* to I_2 produces a population maximum near v=40. LIF survey scans of the D-X bands indicated a population distribution that was consistent with transfer from I*. Populations in levels with v>48 could not be detected. Furthermore, the concentration of $I_2^\dagger$ observed was too low to be consistent with efficient E-V transfer from NCl(a).

NCl(a) is isoelectronic with $O_2(a)$, so it might be expected that these metastables would show comparable E-V transfer probabilities for collisions with I_2. If this were the case, transfer from NCl(a) would be slow ($\approx 10^{-14} cm^3 s^{-1}$), as the present results suggest. It is thought that $O_2(a)$ dissociates I_2 by a chain branching mechanism that depends on I*+I_2 transfer. Even if direct transfer from NCl(a) to I_2 were slow, it likely that a chain branching dissociation mechanism would also be effective for NCl(a).

Photolysis and photoexcitation of I_2 complicated the experiments described here. In future studies we will generate NCl(a) by photolysis of N_3Cl/He mixtures in a flow tube. I_2 will be added to the flow some distance downstream from the photolysis region. Detection of vibrationally and electronically excited products will be accomplished by LIF and REMPI. The design of this apparatus has been completed, and the components are currently being assembled.

7. Spectroscopy of the Br_2 D'-A' ion-pair to valence state transition.

The ion-pair to valence state transitions of the halogens and interhalogens can be used to monitor the participation of metastable states in energy transfer and chemical pumping processes. For this purpose, accurate data for the ion-pair states are required. In recent years we have characterized ion-pair states of I_2 and IBr via laser exciation of jet-cooled metastables. As an ongoing part of this effort, we have applied jet cooling techniques to examine the D'-A' transition of Br_2. This work was motivated, in part, by results obtained at Johns Hopkins University (JHU). While using the photolysis of BBr_3 to seed boron atoms in a free-jet expansion, Prof. Paul Dagdigian and Dr. Eunsook Hwang inadvertently recorded Br_2 D'-A' bands originating from A' v"=0. These spectra were communicated to Prof. Joel Tellinghuisen (Vanderbilt University), who had previously analyzed the emission spectrum[13]. Prof. Tellinghuisen found calibration errors in the JHU spectrum, which precluded the extraction of accurate spectroscopic constants from the extensive data set. Hence, in consultation with Profs. Dagdigian and Tellinghuisen, we undertook a limited study of the Br_2 D'-A' bands at Emory, in order to provide calibration markers for the JHU data.

In the experiments conducted at Emory, jet-cooled $Br_2(A')$ was obtained by electrical discharge excitation of He/Br_2 mixtures in the throat of a pulsed nozzle. Rotationally resolved D'-A' bands were observed by LIF using a frequency doubled dye laser. To discriminate against emissions from the discharge, a small monochromator was used to monitor the LIF at 290 nm. Absolute wavenumber calibration was established by using the fundamental from the dye laser to simultaneously record the spectrum of Te_2. All of the observed Br_2 bands originated from A', v"=0. D' levels in the range $23 \le v' \le 47$ were sampled. Even with jet cooling, the bands were quite congested owing to the presence of three naturally occurring isotopes of Br_2. The overlapping of lines was least troublesome for the $^{79}Br_2$ and $^{79}Br^{81}Br$ isotopes, so the analyses were carried out on these species. Rotational assignments were determined by the method of combination differences. The rotational line positions (υ) were then fit to the standard expression:

$$\upsilon = \upsilon_{v'-v"} + B_{v'}J'(J'+1) - D_{v'}(J'(J'+1))^2 - B_{v"}J"(J"+1) + D_{v"}(J"(J"+1))^2$$

with the centrifugal distortion constants held at the values determined by Sur and Tellinghuisen[13]. The band origins ($\upsilon_{v'-v''}$) and rotational constants resulting from these fits are given in Table 2. The line positions were communicated to Profs. Dagdigian and Tellinghuisen, who used them to calibrate the JHU spectra. A global fit of all of the data for Br_2 D'-A' (including the original emission data of Sur and Tellinghuisen[13]) has been made. Data for all three isotopes were fitted to a mass-weighted Dunham expansion to determine a unique set of molecular constants. For consistency with the earlier studies, we chose $^{79}Br_2$ as the "standard" isotope. Molecular constants resulting from the global fit are listed in Table 3. This work is summarized in reference 14.

8. References

1. T. Van Marter, M. C. Heaven, and D. Plummer, Chem. Phys. Lett. 260, 201 (1996)

2. W. G. Lawrence, T. A. Van Marter, M. L. Nowlin, and M. C. Heaven, Gas and Chemical Lasers: SPIE Proceedings vol. 2702, (1996)

3. W. G. Lawrence, T. A. Van Marter, M. L. Nowlin, and M. C. Heaven, J. Chem. Phys. 106, 127 (1997)

4. M. Kawasaki, H. Sato, and G. Inoue, J. Phys. Chem. 93, 7571 (1989)

5. T. G. Wright, A. Bell, and J. G. Frey, Chem. Phys. Lett. 189, 297 (1992)

6. W. G. Lawrence, R. Fulgum, and M. C. Heaven, J. Phys. Chem. 100, 18702 (1996).

7. A. L. Kaledin, M. C. Heaven, W. G. Lawrence, Q. Cui, J. E. Stevens and K. Morokuma, J. Chem. Phys. Accepted, November 1997

8. J. J. Deakin and D. J. Husain, J. Chem. Soc. Faraday Trans. II 68, 1603 (1972)

9. D. B. Atkinson and M. A. Smith, Rev. Sci. Instrum. 66, 4434 (1995)

10. M. Dolg, H. Stoll, and H. Preuss, J. Chem. Phys. 90, 1730 (1989)

11. G. P. Perram and G. D. Hager, "The standard chemical oxygen iodine laser kinetics package", Air Force Weapons Laboratory, AFWL-TR-88-50, Kirtland AFB, Oct 1988.

12. D. L. Carrol, AIAA J. 33, 1454 (1995)

13. A. Sur and J. Tellinghuisen, J. Mol. Spectrosc. 88, 323 (1981)

14. T. A. Van Marter, Y. Lu, M. C. Heaven, E. Hwang, P. J. Dagdigian and J. Tellinghuisen, J. Mol. Spectrosc. 177, 311 (1996)

TABLE 2

Origins, rotational constants, and rotational variance-covariance matrices from band-by-band least-squares fits of analyzed absorption bands in the $D' - A'$ transition of Br_2.[a]

Species	$v'-v''$	ν_0	$B' \times 100$	$B'' \times 100$	$V_{11} \times 10^9$	$V_{12} \times 10^9$	$V_{22} \times 10^9$
79–79	23–0	38 958.384(9)	3.9079	5.9157	8.39909	8.84580	9.58196
79–79	24–0	39 091.348(7)	3.8625	5.8667	7.19132	7.51421	8.03596
79–79	28–0	39 616.658(11)	3.8391	5.9079	17.25450	17.25450	17.72507
79–79	29–0	39 746.285(8)	3.8187	5.9060	9.39960	9.39960	9.65159
79–79	30–0	39 875.199(8)	3.8033	5.9050	16.91604	16.90035	17.13012
79–79	31–0	40 003.423(8)	3.7742	5.8877	7.94308	8.21983	8.68108
79–79	32–0	40 131.001(5)	3.7750	5.9091	2.93638	2.93638	3.00860
79–79	42–0	41 369.893(7)	3.6231	5.8937	5.85293	5.83024	5.92852
79–79	47–0	41 965.010(8)	3.5250	5.8663	9.35511	9.35511	9.52031
79–81	23–0	38 939.475(7)	3.8545	5.8344	3.49909	3.55612	3.65411
79–81	24–0	39 071.777(8)	3.8541	5.8462	4.79626	4.81161	4.90729
79–81	28–0	39 594.267(10)	3.7870	5.8343	5.31829	5.31829	5.41413
79–81	29–0	39 723.158(7)	3.7814	5.8378	8.36947	8.36947	8.59326
79–81	30–0	39 851.426(5)	3.7575	5.8329	3.79285	3.79285	3.84582
79–81	31–0	39 978.981(5)	3.7462	5.8350	2.18676	2.22797	2.29666
79–81	32–0	40 105.888(5)	3.7306	5.8334	2.94808	2.94808	2.99011
79–81[b]	33–0	40 232.076(8)	3.7260	5.8439	7.68862	7.91577	8.30061
79–81[b]	34–0	40 357.594(9)	3.6798	5.8133	11.37541	11.61895	12.06064
79–81[b]	35–0	40 482.500(10)	3.6969	5.8420	14.51009	14.95115	15.65838
79–81	36–0	40 606.817(6)	3.6622	5.8204	4.07429	4.07429	4.16885
79–81[b]	37–0	40 730.431(13)	3.6446	5.8154	16.11984	16.42306	17.07128
79–81[b]	38–0	40 853.354(12)	3.6353	5.8210	15.50074	15.77899	16.33179
79–81[b]	39–0	40 975.607(11)	3.6112	5.8107	12.01981	12.09435	12.38113
79–81[b]	40–0	41 097.116(14)	3.5750	5.7801	16.09162	16.04227	16.28252
79–81[b]	41–0	41 218.187(10)	3.5722	5.7964	12.83997	12.84631	13.01562
79–81	42–0	41 338.632(6)	3.5859	5.8259	3.75625	3.75625	3.81378
79–81[b]	43–0	41 458.327(10)	3.3174	5.5726	12.77907	13.05129	13.50500
79–81[b]	44–0	41 577.460(9)	3.4309	5.6960	9.35999	9.58455	9.98006
79–81[b]	45–0	41 695.905(11)	3.4184	5.6989	13.11613	13.39959	13.87204
79–81[b]	46–0	41 813.767(11)	3.4454	5.7438	15.99128	16.32984	16.89410
79–81	47–0	41 930.939(6)	3.4716	5.7797	4.84027	4.84027	4.91069

[a]Units cm^{-1} for band origins and rotational constants, cm^{-2} for **V**. In the latter "1" refers to B', "2" to B''.

[b]Bands recorded at Johns Hopkins using BBr_3 photolysis; others recorded at Emory using pulsed electrical discharge source.

TABLE 3

Spectroscopic Parameters (cm^{-1}) for the $D' - A'$ Transition in $^{79}Br_2$[a]

	D'	A'
ΔT_e	35 702.67 (8)	
c_{v0} (T_e)	48 930 (100)	13 230 (100)
c_{v1} (ω_e)	150.860 (8)	162.766 (107)
c_{v2} ($-\omega_e x_e$)	−0.39109 (38)	−1.8416 (462)
c_{v3}	5.78×10^{-4}	−0.0328
c_{v4}	-4.2×10^{-7}	1.754×10^{-3}
c_{v5}		-1.33×10^{-4}
c_{v6}		3.2×10^{-6}
$\mathcal{D}_e$[b]	35 550 (100)	2830 (100)
c_{r0} (B_e)	0.042431 (16)	0.059313 (17)
c_{r1} ($-\alpha_e$)	$-1.494\ (15)\times10^{-4}$	$-5.475\ (51)\times10^{-4}$
c_{r2}	1.7×10^{-7}	-4.8×10^{-6}
c_{r3}	-9×10^{-10}	-6.5×10^{-7}
R_e (Å)	3.1731 (6)	2.6838 (4)
c_{d0} (D_e)[c]	1.343×10^{-8}	3.147×10^{-8}
c_{d1} (β_e)	1.74×10^{-11}	1.1×10^{-9}
c_{d2}	-2.3×10^{-13}	6.44×10^{-11}
c_{d3}		6.1×10^{-12}
c_{d4}		1.2×10^{-13}
c_{h0}[c]	-3.67×10^{-16}	-3.71×10^{-14}
c_{h1}		-8.22×10^{-15}
c_{h2}		6.1×10^{-16}
c_{h3}		-1.15×10^{-16}
c_{h4}		-4.4×10^{-18}
σ[d]	0.083	

[a] From least-squares fit of data (2940 total assignments) for $^{79}Br_2$, $^{79}Br^{81}Br$, and $^{81}Br_2$, spanning $v' = 0$–47 and $v'' = 0$–21. Figures in parentheses for key parameters represent standard errors (1 σ) in terms of final digits. Parameters have been rounded by a systematic procedure that preserves their accuracy.

[b] Dissociation to $Br^-(^1S) + Br^+(^3P_2)$ for D', to two ground-state ($^2P_{3/2}$) atoms for A'.

[c] D_v and H_v parameters fixed at the given values in global fit.

[d] Standard deviation for measurements of unit weight.

9. Publications resulting from AFOSR Support

1. W. G. Lawrence, T. A. Van Marter, M. L. Nowlin, and M. C. Heaven, Gas and Chemical Lasers: SPIE Proceedings vol. 2702, (1996)
"Energy Transfer Mechanisms for $I_2(X)$ in the Chemical Oxygen Iodine Laser"

2. T. A. Van Marter, Y. Lu, M. C. Heaven, E. Hwang, P. J. Dagdigian and J. Tellinghuisen, J. Mol. Spectrosc. 177, 311 (1996)
"Spectroscopy of Metastable Species in a Free-Jet Expansion: The $D' \leftarrow A'$ Transition in Br_2"

3. T. Van Marter, M. C. Heaven, and D. Plummer, Chem. Phys. Lett. 260, 201 (1996)
"Measurement of the Rate Constant for Quenching of $I(^2P_{1/2})$ by O_2 at 150 K"

4. W. G. Lawrence, R. Fulgum, and M. C. Heaven, J. Phys. Chem. 100, 18702 (1996).
"Photolysis of Matrix Isolated HCl-Cl_2 Complexes: Electronic Absorption and Emission Spectra Provisionally Assigned to Cl_3"

5. W. G. Lawrence, T. A. Van Marter, M. L. Nowlin, and M. C. Heaven, J. Chem. Phys. 106, 127 (1997)
"Inelastic Collision Dynamics of Vibrationally Excited $I_2(X)$"

6. A. L. Kaledin, M. C. Heaven, W. G. Lawrence, Q. Cui, J. E. Stevens and K. Morokuma, J. Chem. Phys. Accepted, November 1997
"Ab initio molecular orbital study of the trichlorine radical, Cl_3"